Correlation method for the measure of mask-induced line-edge roughness in extreme ultraviolet lithography

Patrick P. Naulleau

Center for X-Ray Optics, Lawrence Berkeley National Laboratory, Berkeley, CA 94720

Abstract

As critical dimensions for leading-edge semiconductor devices shrink, line-edge roughness (LER) requirements are pushing well into the single digit nanometer regime. At these scales many new sources of LER must be considered. In the case of extreme ultraviolet (EUV) lithography, modeling has shown the lithographic mask to be a source of significant concern. Here we present a correlation-based methodology for experimentally measuring the magnitude of mask contributors to printed LER. The method is applied to recent printing results from a 0.3 numerical aperture EUV microfield exposure tool. The measurements demonstrate that such effects are indeed present and of significant magnitude. The method is also used to explore the effects of illumination coherence and defocus and has been used to verify model-based predictions of mask-induced LER.

Keyword: extreme ultraviolet, lithography, multilayer, mask, line-edge roughness

Introduction

Line edge and width roughness (LER and LWR) remains the most daunting challenge facing the development of commercially viable extreme ultraviolet (EUV) photoresists. LER, however, is not exclusively a resist problem, system-level effects can also be important. Perhaps the most significant of these system level effects for EUV is the mask. [1-4] The mask can contribute to LER in two different ways. The first and most obvious source is from LER on the mask itself. Coupling of the mask LER to the wafer can be understood using the concept of the LER transfer function (LTF) [1] which is closely related to the optic modulation transfer function (MTF). A second, less obvious, source of LER comes from phase roughness in the clear areas of the mask. Because EUV masks are reflective and the wavelength is extremely short, even sub-nm level of roughness can have significant impact on phase roughness in the reflected field. This phase roughness at the mask then couples to the intensity variations at the wafer through the concept of speckle [2,3]. Being a coherent effect, this mask-induced speckle is highly dependent on illumination coherence and defocus.

Recent modeling results [4] have suggested that mask effects are indeed important in advanced EUV development tools such as the SEMATECH Berkeley microfield exposure tool (BMET) [5]. Here we present the first resist-based measurements of such effects. Correlation techniques are used to distinguish mask from resist sources of LER. Moreover, the variable illumination capabilities of the BMET are used to help distinguish the two mask sources of LER. Finally, the experimental results are directly compared to modeling.

Measurement methodology

It is evident that resist sources of LER such as acid shot noise, photo-acid generator uniformity, quencher uniformity, blocking group uniformity, ... will be random from one exposure to the next. Mask sources of LER, however, would be invariant from exposure to exposure. Thus by

characterizing the correlation of the line edge deviation function between multiple exposures of an identical region on the mask we are able to distinguish invariant mask effects from random resist effects. For the purpose of the analysis below, we define L as a random variable representing the deviation of the line edge from a straight line as a function of position along the line. (Note that traditionally we distill this random variable into its standard deviation and report the LER as three times the standard deviation.) Next we represent L as the summation of two independent random variables M and R where M is the mask-induced edge deviation and R is the resist-induced deviation. So for any one exposure, or realization, (represented by subscript i) we write the total measured edge deviation as

$$L_i = M_i + R_i. \tag{1}$$

Because the mask effects are assumed to be invariant all M_i will be completely correlated whereas the random resist deviation realizations R_i will be completely uncorrelated. For the correlated case of M we can drop the subscript and for two independent exposures we get

$$L_1 = M + R_1 \quad , \; L_2 = M + R_2 \, . \tag{2}$$

For further simplification we assume the process to be stationary meaning that statistics are invariant between the individual exposures (realizations), and we assume all the random variables to be zero mean. We note that neither of these assumptions are restrictive. If the statistics were not invariant, characterization of any particular lithography process would be meaningless since it would be different every time, and mean variations of the line edge are not of concern from the perspective of LER

The correlation between L_1 and L_2 can now be written as

$$\rho = \frac{E[L_1 L_2]}{\sigma_{L_1}\sigma_{L_2}} \tag{3}$$

where we have made use of the fact that the variables are zero mean. Expanding the L_1 and L_2 terms and making use of the fact the process is assumed invariant (standard deviation of L_1 and L_2 are the same) yields,

$$\rho = \frac{E[(M + R_1)(M + R_2)]}{\sigma_L^{\,2}} \tag{4}$$

$$\rho = \frac{E[M^2 + R_1 R_2 + M_1 R_2 + M_2 R_1]}{\sigma_L^{\,2}} \tag{5}$$

$$\rho = \frac{E[M^2] + E[R_1 R_2] + E[MR_2] + E[MR_1]}{\sigma_L^{\,2}} \tag{6}$$

Now making use of the fact that M and R as well as individual realizations of R are independent, and again making use of the fact that the variables are zero mean, Eq. 6 simplifies to

$$\rho = \frac{\sigma_M^{\,2}}{\sigma_L^{\,2}} \tag{7}$$

Thus the correlated mask LER (which is proportional to the standard deviation of M) can be written as

$$LER_M = LER_L\sqrt{\rho} \tag{8}$$

where LER_L is the total measured LER.

Experimental results

To experimentally determine the importance of mask effects in recent advanced resist testing with the SEMATECH Berkeley microfield exposure tool [6], we implement the correlation

measurement described above. To accentuate the mask phase roughness effects presented in Section 1, we use a small sigma (0.05) off-axis illumination setting with an offset of 0.65. We refer to this type of illumination as monopole. The use of off axis illumination was required due to the fact that the MET optic [5] used in these tests has a central obscuration with a radius equal to 30% of the total optic pupil. The mask phase roughness effects are further accentuated by working with 100-nm wafer-plane defocus. As demonstrated by the modeled mask-induced LER data in Table 1 (see Ref. [4] for details on the modeling procedure), coherence and defocus parameters have a more significant impact on image LER coupling coming from phase roughness on the mask rather than mask absorber LER. Note that defocus has a more significant impact with annular illumination for both sources of mask-induced LER. This is due to the decreased depth of focus for annular illumination versus monopole. It is interesting to note that based on speckle effects alone one would expect the monopole setting to be more sensitive to defocus for the multilayer roughness case.

Figure 1 shows scanning electron micrographs (SEMs) of three independent exposures of the same 50 nm line on the mask. Although not shown in the images, the line on the mask is positioned in close proximity to a unique alignment feature (label) that is captured within the same SEM image field. Correlation to the alignment feature is used to register the three independent images for analysis. To minimize impact on the results, the alignment accuracy is required to be a fraction of the correlation length of the roughness to be analyzed. As described below, for the results presented here, the correlation length is on the order of 15 nm which is well within the capabilities of the auto-correlation-based alignment procedure. To within the reproducibility of the exposure tool, the illumination and defocus settings are unchanged from image to image, thus we would expect the mask-induced LER to also be unchanged. Focusing on

the bottom edge, Fig. 2 shows the extracted line edge data [7] from the three independent exposures on the same axis. The correlation between the exposures is readily evident by eye. Numerical evaluation of the correlation consists of implementing Eq. 3 where L_1 and L_2 are two of the three sets of line edge data shown in Fig. 2. Doing so yields an average correlation between the three exposures of 61%, where the average correlation is defined as the average of ρ measured from all possible two-line permutations of the three-line data set.

$$\bar{\rho} = (\rho_{1,2} + \rho_{1,3} + \rho_{2,3})/3 \tag{9}$$

The three-line average full LER ($\overline{LER_L}$) for this single edge over the full frequency content present in Fig. 2 is 4.3 nm. Using Eq. 8, the correlated LER ($\overline{LER_M}$) can now be calculated yielding 3.4 ± 0.2 nm.

The uncertainty in the measured correlation number is a function of the total analyzed line length relative the correlation length of the roughness. In essence what is being measured is the cross-correlation of two independent realizations of the line edge. If this line edge is viewed over a length that is short relative to the correlation length of the underlying random processes there will be a very large uncertainty in the measured value unless a large number of independent realizations (exposures) is observed. Assuming the process to be ergodic, a longer length of line can be observed in lieu of a larger number of independent realizations. Clearly the random process of concern arising from random resist and photon effects can be assumed to be ergodic. This being the case, experimental ease strongly favors the use of longer lengths of lines and fewer realizations with the minimum number of realizations as assumed in the analysis above being two. The relative uncertainty of the correlation measurement can be shown to be 1/sqrt(N) where N is the analysis length divided by the correlation length. For the data presented here, the

total analysis length is approximately 1.3 μm and the correlation length and the correlation length approximately 15 nm yielding a relative uncertainty of approximately 10%. The precision is further improved by considering three realizations instead of just two.

Because the projection optics can be viewed as a low-pass filter, one should expect the mask-induced LER to be bandlimited [1,8]. Figure 3 show the power spectral density [7] of the modeled mask-induced LER demonstrating this effect. Figure 3(a) is for mask absorber LER and Fig. 3(b) is for mask multilayer roughness. These results indicate that limiting the bandwidth in our measurement, would cause the correlation to increase since the lowpass filtering will have less effect on the mask-induced LER than resist LER which is not so strongly band limited. Figure 4 shows the filtered line edge data where a tophat filter is used and the cut-off frequency is set to 1/(target pitch), which for this case is 10 μm^{-1}. Note that the cut-off frequency is chosen in accordance to the International Technology Roadmap for Semiconductors [9]. Within this lower frequency range the average correlation is increased to 79% and the average LER decreased to 3.8 nm. Using Eq. 8 the average correlated LER ($\overline{LER_M}$) for the cases in Figs. 2 and 4 respectively is 3.4 ± 0.2 nm where, as described above, the uncertainty is due to the limited extent of the correlation measurement relative to the bandwidth. The fact that $\overline{LER_M}$ remains unchanged while $\overline{LER_L}$ decreases substantially with filtering, shows that as expected due to the low-pass filtering of the optic, the correlated mask-induced LER is found to be significantly more bandlimited than is the uncorrelated resist roughness.

To see how the measured correlated LER ($\overline{LER_M}$) results compare to predicted mask-induced LER values, we perform aerial image modeling with the known imaging conditions and a modeling mask with absorber and phase roughness characteristics statistically matching the

measured mask characteristics [4]. Figure 5 shows the modeled binarized aerial image of 50-nm lines and spaces yielding an average LER of 3.0 over the 12 edges and a 1σ variation for the LER measured on a single edge of 0.7 nm. To within statistical uncertainties, the measured and experimental results are identical.

Next we experimentally explore the effects of lower coherence illumination by performing the same measurement using annular illumination with an inner σ of 0.35 and an outer σ of 0.55. Annular illumination is chosen over a large disk due to the projection optics central obscuration described above. Figure 6 shows the extracted edge overlay plots for both full bandwidth and the bandlimited cases (max frequency = 10 μm^{-1}). The average correlation ($\bar{\rho}$) for the full bandwidth and bandlimited cases are 35% and 60%, respectively. The average LER values ($\overline{LER_L}$) are 4.3 nm and 3.6 nm, respectively. The values lead to correlated LER magnitudes ($\overline{LER_M}$) of 2.5 ± 0.3 nm and 2.8 ± 0.3 nm, respectively. The modeling for this case (Fig. 7) yields a predicted mask-induced LER of 2.5 ± 0.3 nm for a single edge. Using the modeling data in Table 1 as a guide, the fact that the correlated roughness decreased by going to annular illumination indicates that mask multilayer roughness is the dominant source of the measured correlated LER. The values in Table 1 can be explained heuristically by noting that mask multilayer roughness leads to LER through the generation of speckle by virtue of the random phase it imparts on the reflected beam. It is evident that this speckle effect becomes increasingly severe as coherence is increased. For mask absorber pattern roughness, however, the trend is the opposite due to the improved imaging characteristics for the annular illumination compared to the small σ off axis case. Should the correlated LER have been found to increase when going to annular illumination, the conclusion would have been that the dominant mask

effect is the absorber LER instead of the multilayer roughness.

Finally we experimentally consider the effect of defocus with annular illumination. Figure 8 shows the extracted edge overlay plots for both full bandwidth and the bandlimited cases (max frequency = 10 μm^{-1}) at best focus. The average correlation ($\bar{\rho}$) for the full bandwidth and bandlimited cases are 35% and 53%, respectively. The average LER values ($\overline{LER_L}$) are 3.5 nm and 2.7 nm, respectively. The values lead to correlated LER magnitudes ($\overline{LER_M}$) of 2.1 ± 0.3 nm and 2.0 ± 0.3 nm, respectively. The modeling for this case (Fig. 9) yields a predicted mask-induced LER of 1.4 ± 0.3 nm for a single edge. Although very close to still having overlapping error bars between measurement and prediction, the match is clearly not as good as the other two cases. The discrepancy could come from an experimental error in the focus setting. For example, the experimental focus step size was 100 nm which arguably could lead to a focus error of 50 nm. Another potential source of effective focus error is from the finite thickness of the resist making it physically impossible to achieve the ideal planar focus value. Note that the film thickness for these measurements was 80 nm which is significant compared to the 100-nm focus change of interest. Figure 10 demonstrates the modeled sensitivity of the process to defocus. Plotted is the modeled mask-induced LER for the conditions in Fig. 9 but for variable focus.

Although the above results are focused on determining the correlated LER ($\overline{LER_M}$), it is evident that the same process also yields a measure of the uncorrelated LER

$$LER_R = LER_L\sqrt{1-\rho}$$

which can be interpreted to represent the resist-limited LER. Table 2 shows the uncorrelated

LER ($\overline{LER_R}$) for the three cases described above along with the modeled image log slope. As expected, the resist-limited LER is inversely proportional to the image log slope in cases where the image log slope drops below 85 μm^{-1}. Despite the sizable mask contributions found above, the resist-limited LER itself remains of significant concern due to the quadratic nature of the addition of the two terms.

Summary

A exposure-to-exposure correlation procedure has been presented allowing resist-image LER to be segregated into correlated and uncorrelated terms. The correlated terms, being fixed in time, are attributed to mask effects and the uncorrelated terms assumed to be due to random resist and shot noise effects. Moreover, by applying the method with various illumination and focus settings, the two dominant mask contributors (absorber LER and multilayer roughness) can further be distinguished. This methodology provides crucial insight for targeting future LER reduction efforts. The method has been used to determine the dominant LER effects in prints from a high resolution EUV microfield exposure research and development tool. The correlation measurement has successfully verified predicted mask-induced LER effects. As expected based on detailed metrology of the mask and modeling, mask multilayer roughness has been shown to be the dominant effect for our experimental conditions. The effects are highly dependent on illumination coherence and defocus. The method can also be applied to measure the resist-limited (uncorrelated) LER allowing resist researchers to better understand the fundamental limits of their materials.

The author is greatly indebted to Paul Denham, Brian Hoef, Gideon Jones, and Lorie Mae Baclea-an for expert support with the exposure tool, and to the entire CXRO staff for enabling this research. The author is also grateful to Warren Montgomery, Chawon Koh, Stefan Wurm, and Brian Rice of SEMATECH for program support. This work was supported by SEMATECH

and carried out at Lawrence Berkeley National Laboratory's Advanced Light Source, which is supported by the Director, Office of Science, of the U.S. Department of Energy under Contract No. DE-AC02-05CH11231.

References

1. P. Naulleau and G. Gallatin, "The line-edge roughness transfer function and its application to determining mask effects in EUV resist characterization," Appl. Opt. **42**, 3390-3397 (2003).

2. N. Beaudry, T. Milster, "Effects of mask roughness and condenser scattering in EUVL systems," Proc. SPIE. **3676**, 653-662 (1999).

3. P. Naulleau, "The relevance of mask-roughness-induced printed line-edge roughness in recent and future EUV lithography tests," Appl. Opt. **43**, 4025-4032 (2004).

4. P. Naulleau, D. Niakoula, G. Zhang, "System-level line-edge roughness limits in extreme ultraviolet lithography," J. Vac. Sci. & Technol. B **26**, 1289-1293 (2008).

5. P. Naulleau, K. Goldberg, E. Anderson, K. Bradley, R. Delano, P. Denham, B. Gunion, B. Harteneck, B. Hoef, H. Huang, K. Jackson, G. Jones, D. Kemp, A. Liddle, R. Oort, A. Rawlins, S. Rekawa, F. Salmassi, R. Tackaberry, C. Chung, L. Hale, D. Phillion, G. Sommargren, J. Taylor, "Status of EUV microexposure capabilities at the ALS using the 0.3-NA MET optic," Proc. SPIE **5374**, 881-891 (2004)..

6. P. Naulleau, C. Anderson, J. Chiu, P. Denham, S. George, K. Goldberg, M. Goldstein, B. Hoef, R. Hudyma, G. Jones, C. Koh, B. La Fontaine, A. Ma, W. Montgomery, D. Niakoula, J. Park, T. Wallow, S. Wurm, "22-nm half-pitch extreme ultraviolet node development at the SEMATECH Berkeley microfield exposure tool," *to be published*, Micro. Eng. (2009).

7. SuMMIT

8. P. Naulleau and G. Gallatin, "Spatial scaling metrics of mask-induced induced line-edge roughness," J. Vac. Sci. & Technol. B, *to be published* (2008).

9. International Technology Roadmap for Semiconductors, 2006 Update, (http://www.itrs.net/Links/2008ITRS/Home2008.htm)

List of Figures

Fig. 10. Modeled sensitivity of the process to defocus. Plotted is the modeled mask-induced LER for the conditions in Fig. 9 but for variable focus.

List of Figures

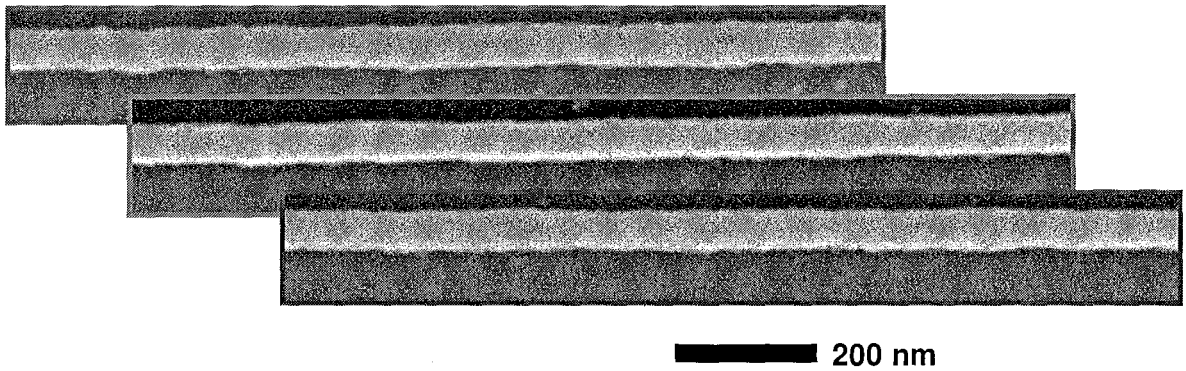
200 nm

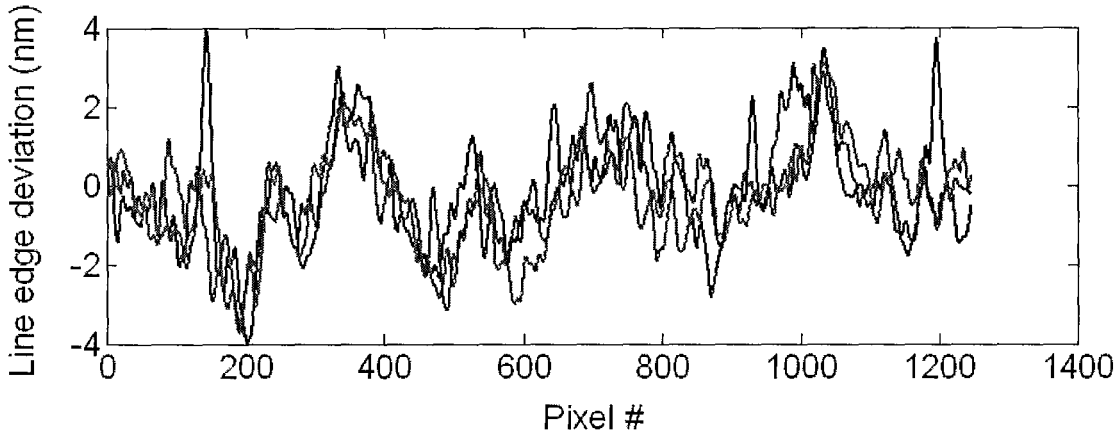
Line edge deviation (nm)
4
2
0
-2
-4
0
200
400
600
800
1000
1200
1400
Pixel #

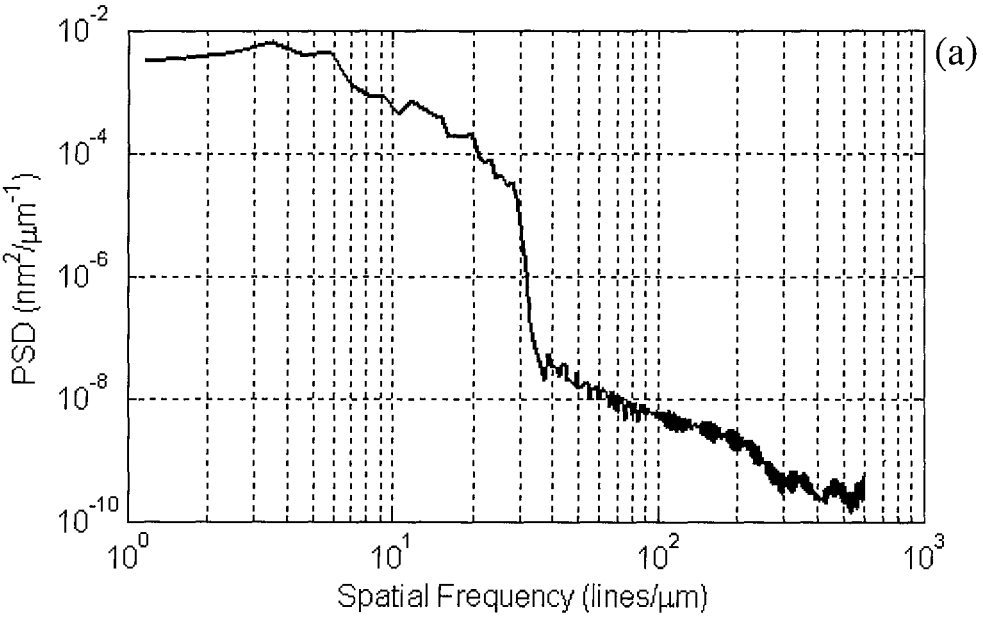
(a)
PSD (nm²/μm⁻¹)
10⁻²
10⁻⁴
10⁻⁶
10⁻⁸
10⁻¹⁰
10⁰
10¹
10²
10³
Spatial Frequency (lines/μm)

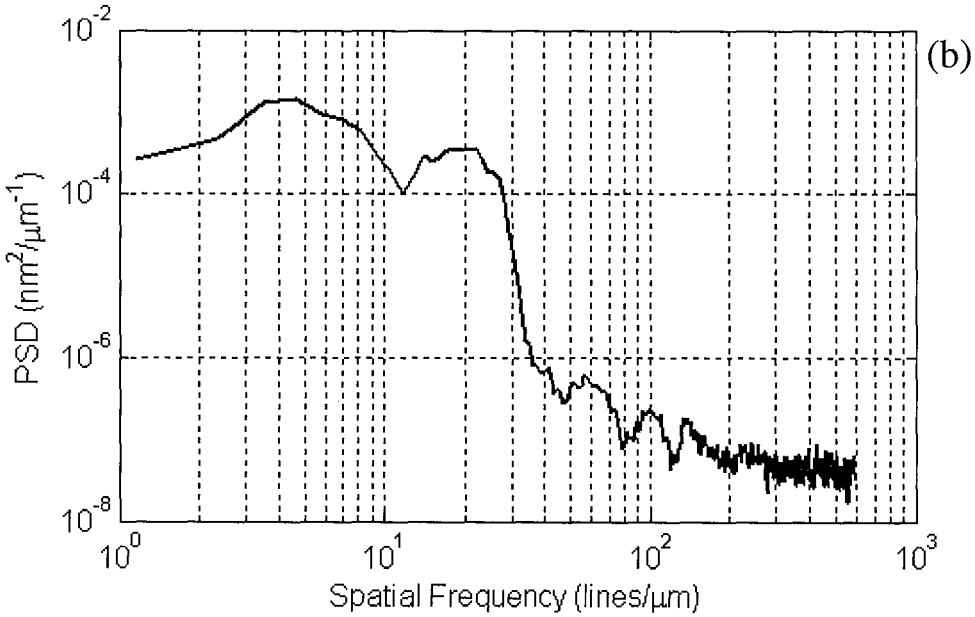
(b)
PSD (nm²/μm⁻¹)
10⁻²
10⁻⁴
10⁻⁶
10⁻⁸
10⁰
10¹
10²
10³
Spatial Frequency (lines/μm)

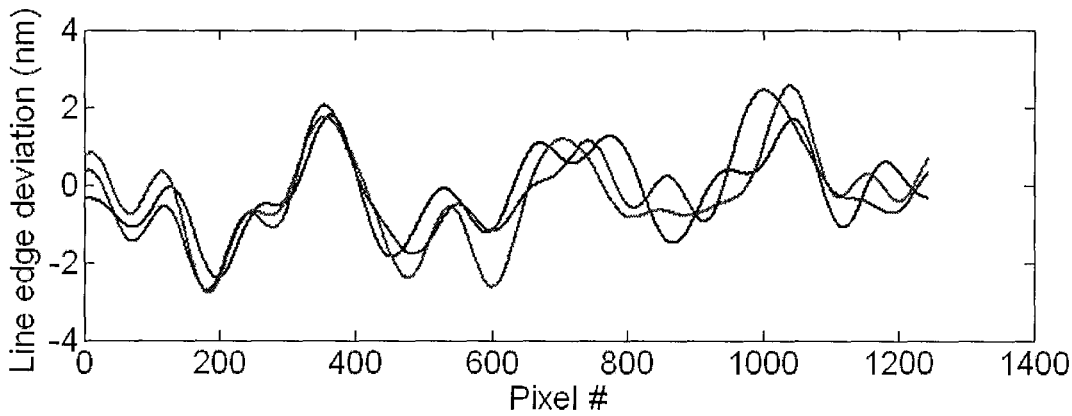
Line edge deviation (nm)
4
2
0
-2
-4
0
200
400
600
800
1000
1200
1400
Pixel #

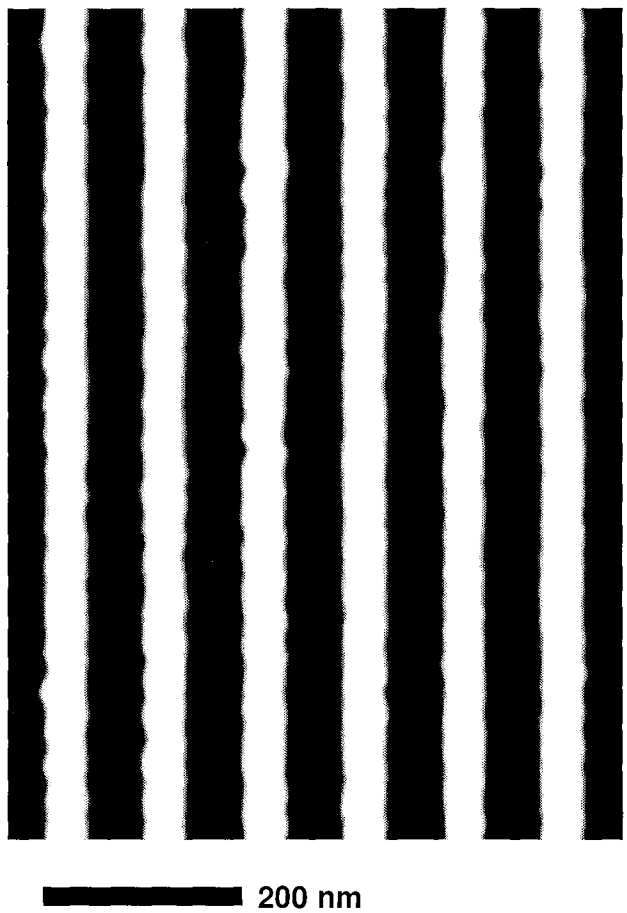
200 nm

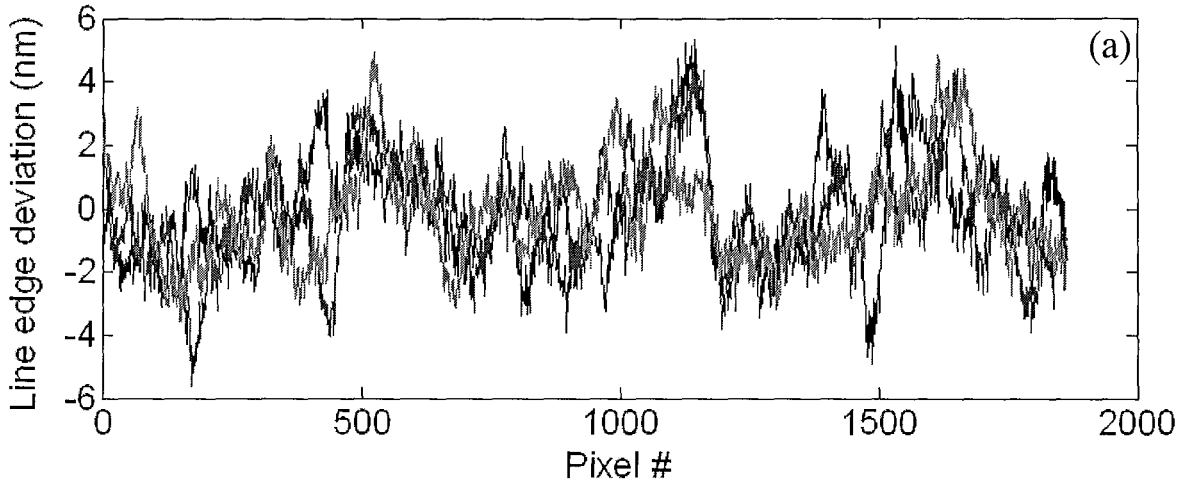
(a)
Line edge deviation (nm)
6
4
2
0
-2
-4
-6
0
500
1000
1500
2000
Pixel #

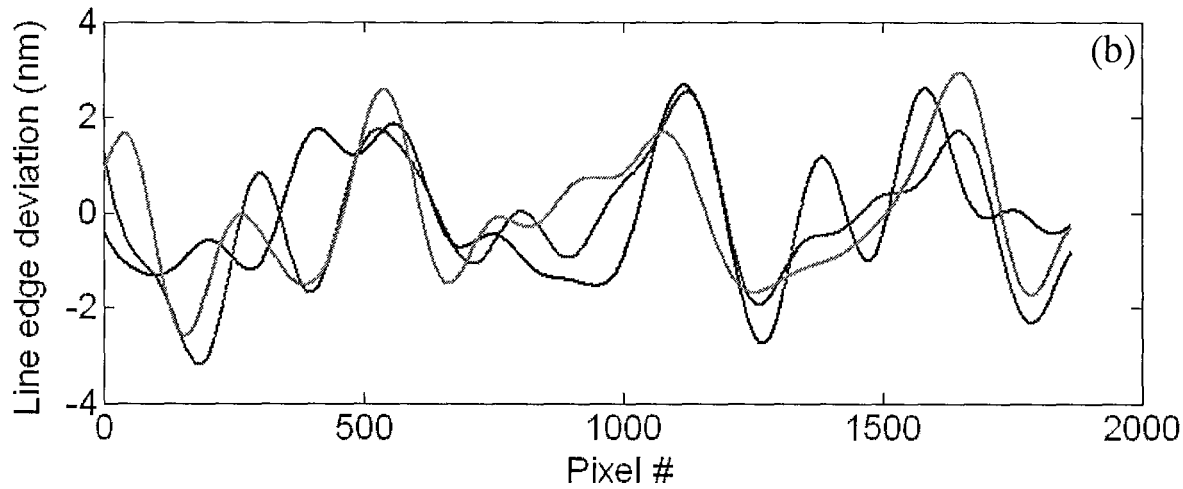
(b)
Line edge deviation (nm)
4
2
0
-2
-4
0
500
1000
1500
2000
Pixel #

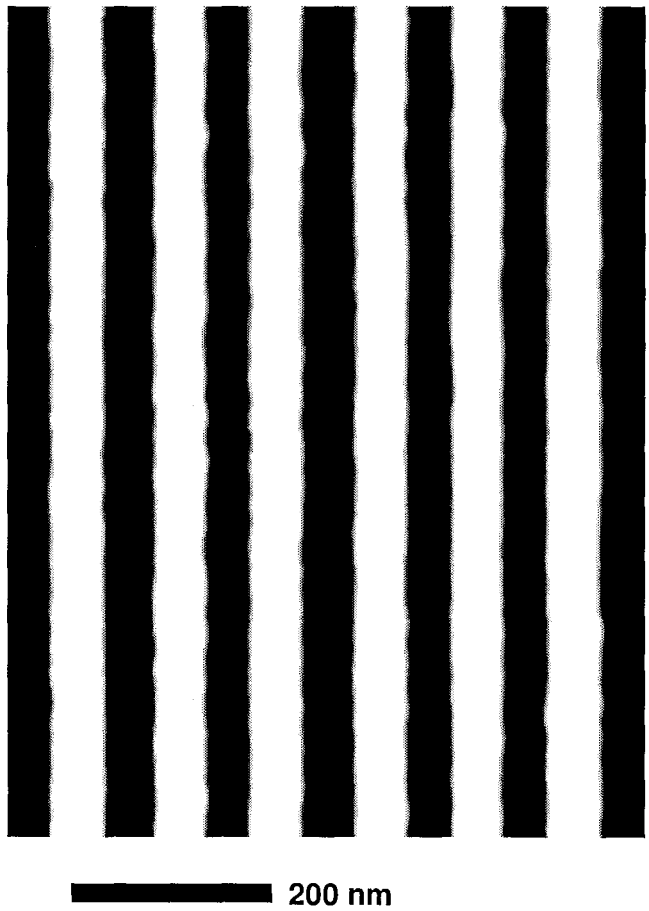
200 nm

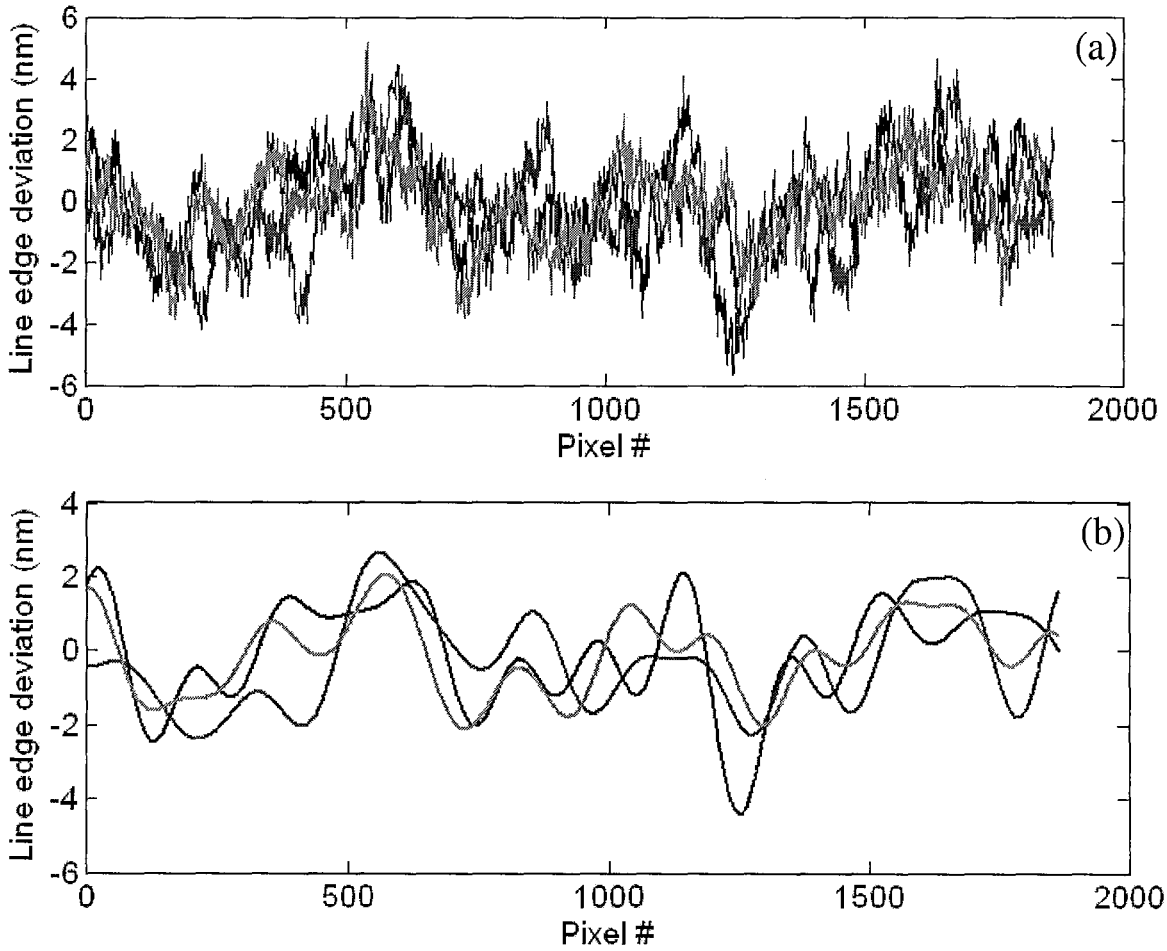
(a)
Line edge deviation (nm)
6
4
2
0
-2
-4
-6
0
500
1000
1500
2000
Pixel #
(b)
Line edge deviation (nm)
4
2
0
-2
-4
-6
0
500
1000
1500
2000
Pixel #

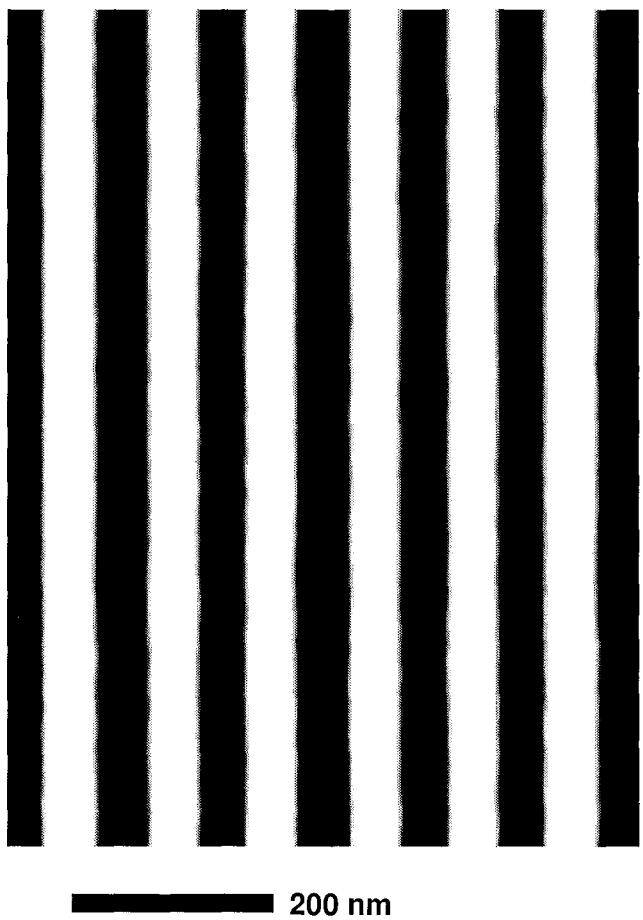
200 nm

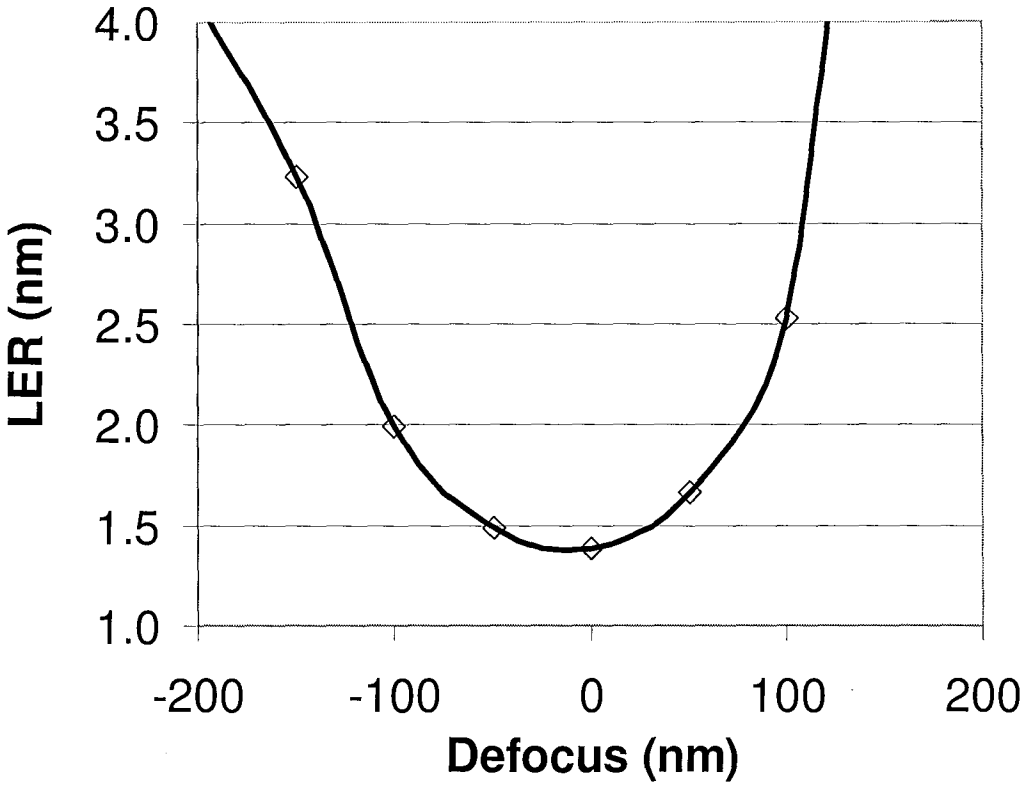
4.0
3.5
3.0
2.5
2.0
1.5
1.0
LER (nm)
-200
-100
0
100
200
Defocus (nm)

	Annular		Monopole σ = 0.05	
	Best focus	100-nm defocus	Best focus	100-nm defocus
Absorber LER	1.20	1.27	0.74	0.81
Multilayer roughness	0.85	1.84	2.63	2.93

	Uncorrelated LER (nm)	Image log slope (μm^{-1})
Monopole, 100-nm defocus	2.7	120
Annular, 100-nm defocus	3.5	65
Annular, best focus	2.8	85